# Raman scattering of mixed $K_{1-x}Na_xCl$ crystals



1989 J. Phys.: Condens. Matter 1 1381

(http://iopscience.iop.org/0953-8984/1/8/001)

J. Phys.: Condens. Matter 1 (1989) 1381–1394. Printed in the UK

# Raman scattering of mixed $K_{1-x}Na_xCl$ crystals

Christina Hilbert†‡, Dieter Strauch†, Takeshi Miyanaga§‖ and Fritz Luty§¶

† Institut für Theoretische Physik, Universität Regensburg, D-8400 Regensburg, Federal Republic of Germany

§ Physics Department, University of Utah, Salt Lake City, Utah 84112, USA

Received 29 January 1988, in final form 25 July 1988

**Abstract.** Raman scattering for $Na_xK_{1-x}Cl$ single crystals with 12 different Na concentrations $x$ has been measured at 300 and 10 K. The cationic-disorder-induced Raman effect in the one-phonon region 0–200 $cm^{-1}$ has been experimentally analysed in terms of spectral structure, symmetry and relative strength as a function of Na concentration $x$. For low concentrations (3–6%) of $Na^+$ or $K^+$ single defects or defect pairs, theoretical calculations have been performed based on the semi-classical off-resonance theory with a Green function–breathing shell model approach in the average $T$-matrix approximation. The agreement between calculated and experimental spectra can be considerably improved by basing the model on inter-ionic (rather than intra-ionic) polarisability and by extending coupling and force-constant changes beyond the first to second and fourth neighbours of the defect. Some serious discrepancies, however, remain unresolved.

## 1. Introduction

In this paper, we present an experimental and theoretical study of the first-order impurity-induced Raman scattering of mixed $Na_xK_{1-x}Cl$ crystals. Pure crystals with a rocksalt structure in which every site is at a centre of inversion do not show first-order scattering. One can observe only a continuous second-order spectrum. When a substitutional impurity is introduced into an alkali halide, the loss of the inversion symmetry for all atoms except the defect itself allows first-order Raman scattering. This is a consequence of the fact that only modes which transform as a second-rank tensor under the point-group operations of the space group will be Raman active. If inversion is an operation of the crystal point group, only even-parity modes take part in the scattering process. In § 2 the experimental arrangement and results are displayed. The Raman scattering spectra have been obtained at 300 and 10 K for various compositions of the mixed crystals and have been analysed in terms of their symmetry. Similar experiments have already been performed on $KBr_{1-x}I_x$, $KCl_{1-x}I_x$ and $K_{1-x}Rb_xCl$ crystals by Nair and Walker (1973); however, the spectra, taken mostly at room temperature, show relatively little detail.

In § 3 a short review of the theory is given. Our calculations are based on the

‡ Present address: GPP, Kolpingring 18a, 8024 Oberhaching, Federal Republic of Germany.

‖ Present address: Physics Department, Faculty of Education, Wakayama University, Wakayama, Japan.

¶ To whom reprint requests should be addressed.

0953-8984/89/081381 + 14 $02.50 

semi-classical off-resonance theory of Born and Huang (1954), Maradudin (1966) and Benedek and Nardelli (1967). For further reviews see, e.g., Barker and Sievers (1975) and Bilz *et al* (1984). In § 4 the theoretical results for the crystals with low defect concentrations are discussed and compared with the experimental spectra.

## 2. Experimental techniques and results

Mixed $Na_xK_{1-x}Cl$ crystals were grown in the Utah Crystal Growth Laboratory from various mixtures of reagent-grade KCl and NaCl by the Czochralski technique under a pure Ar atmosphere. The actual Na and K concentrations in the crystal (different from the melt concentrations) were determined by atomic spectroscopy analysis. Mixed crystals of a single composition phase can be formed by slow cooling to room temperature only in the range of rather small Na 'impurity concentrations' (i.e. $0 \leqslant x \leqslant 0.15$) or rather small K 'impurity concentrations' (i.e. $0.92 \leqslant x \leqslant 1.0$). In all the middle region of more equally mixed cation combinations ($0.15 < x < 0.92$), a single solid solution exists only at high temperatures. Under slow cooling below about 450 °C, it separates into domains of the two above-mentioned Na- and K-rich phases, producing—owing to the different refractive indices of the two compositions—an opaque crystal. However, we succeeded by rapid thermal quenching (directly from the crystal growth apparatus)

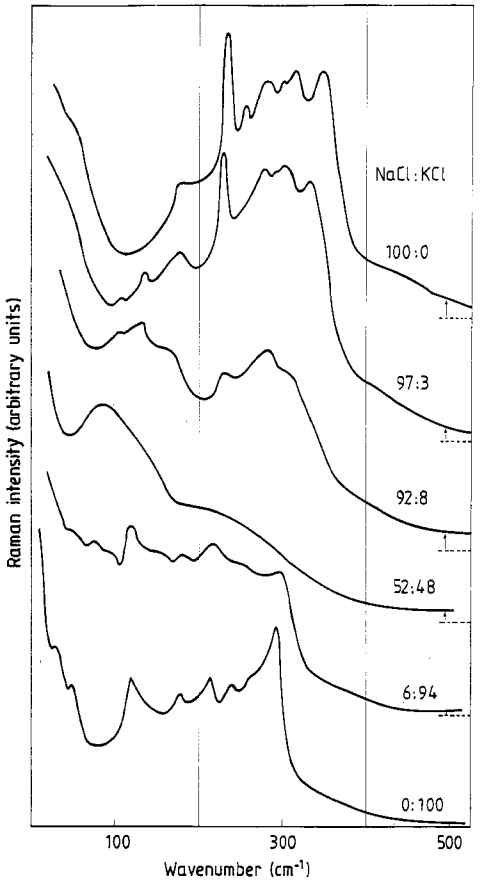


**Figure 1.** Raman spectra of NaCl : KCl mixed crystals, measured at 300 K without analysis of its polarisation under excitation with (110) polarised 5145 Å laser light. Note that the spectra are not to equal scale and cannot be directly compared.

from 550 °C to room temperature, to avoid this phase separation and to produce small transparent crystals of frozen-in single composition phase $Na_{0.52}K_{0.48}Cl$.

The measurements were performed using $\lambda = 5145$ Å excitation with a Spectra Physics 171 $Ar^+$ laser and detection of the Raman scattered light in the usual direction perpendicular to the excitation light, using a Spex 1402 double-grating monochromator and an Ortec 9315 photon-counting system with cooled RCA C-31034 photomultiplier.

Figure 1 and 2 summarise the Raman spectra of $Na_xK_{1-x}Cl$ mixed crystals, obtained under incident polarised $\boldsymbol{E}_i \| \langle 110 \rangle$ laser light at 300 K (figure 1), and for $\boldsymbol{E}_i \| \langle 100 \rangle$ light at 10 K (figure 2). As in both cases the scattered light intensity was measured unpolarised, the spectra contain all symmetries of the Raman-active modes of the crystals. By using five geometries for the $\boldsymbol{E}$-vector of the incident and scattered light, we can separate the Raman spectra into the three symmetries $A_{1g}$, $E_g$ and $T_{2g}$ (referring to the three irreducible representations of the point group $O_h$ of a single defect).

(i) $\langle 100 \rangle \langle 100 \rangle$ yields $A_{1g} + E_g$ spectra.
(ii) $\langle 100 \rangle \langle 010 \rangle$ yields $\frac{1}{2}T_{2g}$ spectra.
(iii) $\langle 110 \rangle \langle 110 \rangle$ yields $A_{1g} + \frac{1}{4}E_g + \frac{1}{2}T_g$ spectra.
(iv) $\langle 1\bar{1}0 \rangle \langle 110 \rangle$ yields $\frac{3}{4}E_g$ spectra.
(v) $\langle 110 \rangle \langle 001 \rangle$ yields $\frac{1}{2}T_{2g}$ spectra.

For a properly oriented crystal, the last three geometries can be realised by varying only the light polarisation without moving the crystal, thus yielding in a single experiment three Raman spectra from which the symmetries and their relative strengths can be easily obtained. Additional measurements of $\langle 100 \rangle$ cleaved crystals using the simple geometries (i) and (ii) provided more polarised spectra than needed for the analysis and were completely consistent with the data from the last three geometries. The spectra of six of the twelve crystals of different $x$ values (shown in figure 2) were symmetry analysed in this way at 10 K, with a result illustrated in figure 3 for five typical selected crystals. While the monovalent cationic impurities in alkali halides (such as $Tl^+$, $Ag^+$, $Cs^+$ and $Rb^+$ in KCl) studied so far induce Raman spectra of only $E_g$ and $T_{2g}$ symmetry (Harley *et al* 1971, Nair and Walker 1973, Höner zu Siederdissen 1976), $NaCl:K^+$ and $KCl:Na^+$ are unique in yielding Raman spectra of all three symmetries.

The top and bottom curves in both figure 2 and figure 3 show the well known second-order Raman spectra of pure NaCl and KCl, occurring at low temperatures essentially in the approximate two-phonon range 100–400 $cm^{-1}$. Gradual introduction of $K^+$ and $Na^+$ impurities into these two hosts produces various Raman bands in the 50–200 $cm^{-1}$ one-phonon spectral range with increasing strength. As the symmetry analysis shows (illustrated in figure 3), the most prominent effect appears in $E_g$ symmetry, with the main peak for $Na^+$ impurities in KCl at 80 $cm^{-1}$, and for $K^+$ impurities in NaCl with the main peak of a multi-band structure at about 120 $cm^{-1}$. Next in relative strength are $A_{1g}$ effects, with a single sharp band at 195 $cm^{-1}$ for $K^+$ impurities in NaCl, and bands in the 80 and 220 $cm^{-1}$ range for $Na^+$ impurities in KCl. Least in strength are $T_{2g}$ effects, which occur for both defect systems rather unstructured in the 50–200 $cm^{-1}$ range.

The question of how the strength of these defect-induced Raman bands depend on this concentration $x$ or $1 - x$ is essential for the theoretical interpretation. We tested it carefully in two different ways.

(a) Leaving the experimental set-up and parameters (such as laser geometry and intensity, cryostat, light collection, spectral slit width and detection sensitivity) exactly the same and exchanging only the crystals (of equal size and surface quality) to be measured should allow direct comparison of the absolute intensities of their Raman

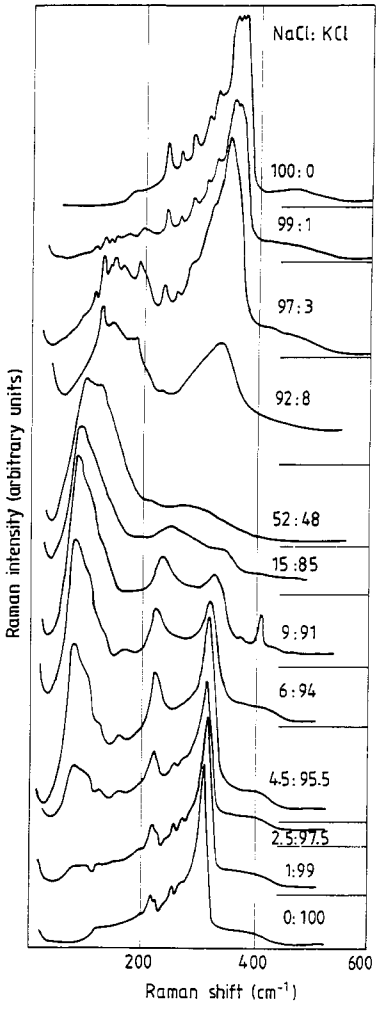


**Figure 2.** Raman spectra of NaCl : KCl mixed crystals, measured at 10 K without analysis of its polarisation under excitation with ⟨100⟩ polarised 5145 Å laser light.

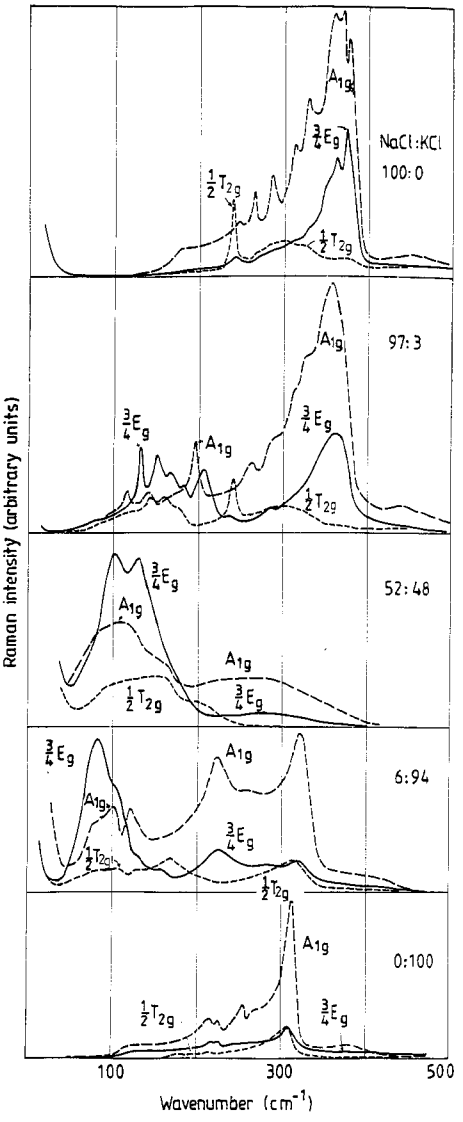


**Figure 3.** Low-temperature (10 K) Raman spectra of mixed NaCl : KCl crystals, separated into the three symmetries $A_{1g}$, $\frac{1}{2}T_{2g}$ and $\frac{3}{4}E_g$. (The raw data were obtained in three scattering geometries $\langle E_i\rangle\langle E_{sc}\rangle$ = ⟨110⟩⟨110⟩, ⟨110⟩⟨001⟩ and ⟨1$\bar{1}$0⟩⟨110⟩.)

response. (Some of the spectra were taken with values of laser intensity and slit height different from the standard values of these parameters. The intensities of these spectra were normalised by multiplying factors to correct the differences in laser intensity and slit height.)

(b) For small impurity concentration (less than 10%) the pronounced second-order Raman peak of the hosts (at about 320 $cm^{-1}$ and about 370 $cm^{-1}$ in KCl and NaCl) should—besides an impurity-induced broadening effect—remain basically unchanged in its integrated Raman intensity. Therefore the ratio of the defect-induced Raman

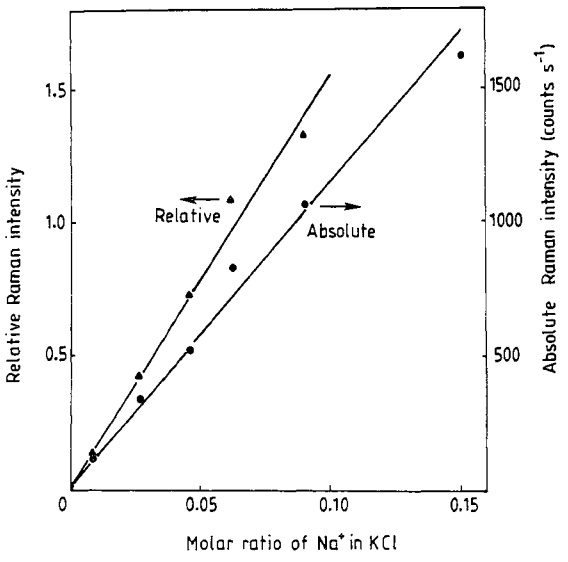


**Figure 4.** Intensity of the Raman peak at 80 $cm^{-1}$ as a function of the $Na^+$ doping in KCl, measured absolutely by direct comparison of different measurements (●, right-hand scale) and relatively to the integrated two-phonon Raman peak around 300 $cm^{-1}$ (▲, left-hand scale).

signal to this constant 'reference value' will yield a reliable Raman strength calibration for different $x$ values (independent of variations in the experimental conditions).

Figure 4 shows the 80 $cm^{-1}$ Raman strength for KCl pure and doped with six different $Na^+$ concentrations $x$, determined with both the 'absolute' (a) and the 'relative' (b) techniques. In both cases a linear dependence on $x$ results within experimental accuracy ($\pm 10\%$), demonstrating that the more simple absolute comparison technique (a) is very reliable and can be extended over the whole $0 \leqslant x \leqslant 1$ concentration range.

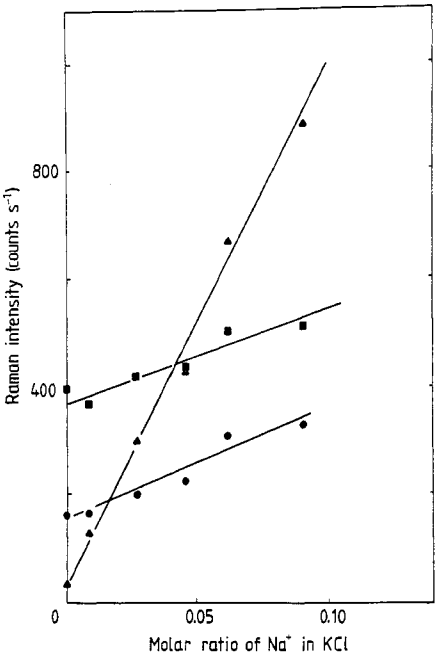


**Figure 5.** Intensities of three $Na^+$-induced Raman peaks as a function of the $Na^+$ doping in KCl: ▲, 102 $cm^{-1}$; ●, 160 $cm^{-1}$; ■, 220 $cm^{-1}$.

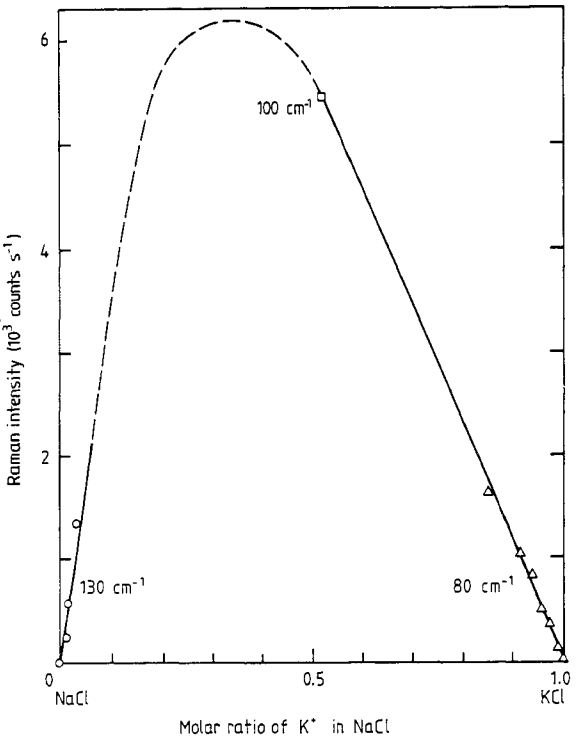


**Figure 6.** Intensity variation of the main $E_g$ one-phonon peak measured and extrapolated over the whole composition range of the NaCl : KCl mixed system..

Figure 5 shows the absolute Raman intensity of the 102, 160 and 220 $cm^{-1}$ band, measured in KCl as a function of $Na^+$ impurity concentration. Again linear scaling is observed in all three cases, although the last one occurs on top of a background second-order Raman signal of the pure KCl host (see discussion later). Similar measurements in the NaCl host show a linear dependence on small $K^+$ impurity concentrations, as illustrated for the 130 $cm^{-1}$ Raman band in figure 6.

In summary the Raman response in the 0–200 $cm^{-1}$ range, scaling in strength linearly with impurity concentration, represents very probably one-phonon Raman spectra of $A_{1g}$, $E_g$ and $T_{2g}$ symmetry, induced by single $Na^+$ or $K^+$ defects. This interpretation, however, is questionable for the 220 $cm^{-1}$ band, which lies slightly above the one-phonon cut-off for KCl and is already present with appreciable strength and with the same $A_{1g} : E_g \simeq 3 : 1$ intensity ratio in pure KCl (see figures 2 and 3). In this latter system it cannot be caused by unavoidable small Na concentrations, because all the other one-phonon Raman bands, scaling with Na contents, are totally absent. Therefore it is definitely a second-order Raman effect in pure KCl. Its linear increase with increase in Na doping (see figures 2, 3 and 5) could suggest that isolated $Na^+$ impurities increase the strength of this particular second-order Raman peak of pure KCl—a challenge for the theory to justify and interpret.

The presence of at least one totally disordered crystal in the middle of the mixture ($x = 0.52$) allows us comparison with the pure crystals with dilute $Na^+$ or $K^+$ defects. Although these two types of system are physically quite different, amazing similarities in the one-phonon Raman response can be established from our data.

(1) The main *peak position* (at 80 $cm^{-1}$ and 120 $cm^{-1}$ for dilute $Na^+$ and $K^+$ defects, respectively) shifts gradually through the mixture, reaching about 100 $cm^{-1}$ in the middle

(see figure 2). The *spectral fine structure* observed at the 'defect ends' washes out in the middle of the mixture, as one might expect.

(2) The essential *symmetry behaviour*, similar for both $Na^+$ and $K^+$ defects with the strength relation $I(E_g) > I(A_{1g}) > I(T_{2g})$ remains well preserved in the totally disordered mixture, as seen easily in figure 3.

(3) The *total strength*, scaling linearly with cationic defect concentration at both ends of the mixture, extrapolates very well from the KCl side to the midpoint of the mixture (full curve). Further extrapolation towards the NaCl side (broken curve) is of course rather arbitrary. Figure 6 shows this behaviour, using measurements of the (unpolarised) intensity of the one-phonon Raman peak through the mixture, using the 'absolute comparison technique' introduced earlier.

This simple preservation or monotonic shift of the essential one-phonon Raman properties (peak position, symmetry and specific strength) thoughout the mixture suggests that certain connections should exist between theoretical treatment of isolated defects and that of the totally disordered crystal.

## 3. Theory

In the following section a short outline of the theory is given. A more detailed derivation can be found in the article by Harley *et al* (1971).

For off-resonance the intensity of linearly polarised Raman scattering per unit solid angle and per unit frequency is given by Born and Huang (1954):

$$I(\omega_s) = \frac{\omega_i^4}{2\pi c^3} \sum_{\alpha\beta\gamma\lambda} n_\alpha n_\beta i_{\alpha\gamma,\beta\lambda}(\omega) E_\gamma(\omega_i) E_\lambda^*(\omega_i). \tag{1}$$

$\omega = \omega_s - \omega_i$ is the frequency difference between scattered and incident radiation, $n_\alpha$ is the $\alpha$-component of the unit vector parallel to the scattered electric field and $E_\gamma(\omega_i)$ is the $\gamma$-component of the incident field.

The Raman scattering tensor is given by

$$i_{\alpha\gamma,\beta\lambda}(\omega) = \frac{1}{2\pi} \int_{-\infty}^{+\infty} d\tau \exp(-i\omega\tau) \langle P_{\alpha\gamma}^\dagger(\boldsymbol{u}, \tau) P_{\beta\lambda}(\boldsymbol{u}) \rangle. \tag{2}$$

$P_{\beta\lambda}(\boldsymbol{u})$ is the operator for the static electronic polarisability of the crystal in its electronic ground state and for a fixed nuclear configuration $\boldsymbol{u}$, and $P_{\alpha\gamma}(\boldsymbol{u}, \tau)$ is the interaction representation of $P_{\alpha\gamma}(\boldsymbol{u})$. In the harmonic approximation the Stokes component of the scattering tensor for first-order Raman scattering can be written in the form

$$i_{\alpha\gamma,\beta\lambda}(\omega) = \hbar \sum_f \frac{1}{2\omega_f} P_{\alpha\gamma,f} P_{\beta\lambda,f} \eta(\omega_f) \delta(\omega + \omega_f) \tag{3}$$

with

$$\eta(\omega) = [1 - \exp(-\beta h\omega)]^{-1}$$

and coupling constants

$$P_{\alpha\gamma,f} = \partial P_{\alpha\gamma}(\boldsymbol{u}) / \partial d_f.$$

$d_f$ are the normal coordinates of the system which are related through the eigenvectors $\boldsymbol{\chi}(f)$ to the vectors $\boldsymbol{u}$ containing the displacements of the lattice particles from the equilibrium position by

$$\boldsymbol{u} = \sum_f \boldsymbol{\chi}(f) d_f.$$

**Table 1.** Representations of Raman-active modes.

| Defect configuration | Point group | 'Raman'-active representation |
|---|---|---|
| Single defect | $O_h$ | $A_{1g}, E_g, T_{2g}$ |
| Defect pair [100] | $D_{4h}$ | $A_{1g}, B_{1g}, B_{2g}, E_g$ |
| Defect pair [110] | $D_{2h}$ | $A_{1g}, B_{1g}, B_{2g}, B_{3g}$ |

Comparing the expansion of $P_{\alpha\gamma}(\boldsymbol{u})$ in terms of the particle displacements $\boldsymbol{u}$ with the expansion in terms of the normal coordinates $d_f$, one obtains the following relation between the first-order coupling coefficients:

$$P_{\alpha\beta,f} = \sum_{m\gamma} P_{\alpha\beta}(m\gamma)\chi(m\gamma|f) =: \mathcal{P}^{\mathrm{T}}_{\alpha\beta}\boldsymbol{\chi}(f). \tag{4}$$

$\chi(m\gamma|f)$ is the $(m\gamma)$ component of $\boldsymbol{\chi}(f)$, $\gamma$ is equal to $x$, $y$ or $z$, and $m$ runs over all $N$ atoms of the crystal.

Group theoretical considerations leads to certain selection rules; only those $\boldsymbol{\chi}(f)$ contribute to first-order Raman scattering which belong to a representation contained in $T_{1u} \times T_{1u}$.

Using the fact that $\mathcal{P}_{\alpha\beta}$ is a symmetric tensor, one obtains the representations of the Raman-active modes shown in table 1. A special result is that only modes with even parity contribute to the scattering process. Therefore the spectra for a point defect are independent of the ionic mass change, in contrast with the spectra from the defect pairs.

In terms of the harmonic phonon Green function matrix $\mathbf{G}(z)$ the Stokes component to the scattering tensor can be written as

$$i_{\alpha\gamma,\beta\lambda}(-|\omega|) = (1/\pi)\hbar\eta(|\omega|)\,\mathrm{Im}[\mathcal{P}^{\mathrm{T}}_{\alpha\gamma}\mathbf{G}(z)\mathcal{P}_{\beta\lambda}]$$

with $z = \omega^2 + \mathrm{i}\varepsilon$ and the limit $\varepsilon \to 0^+$ being understood.

The final step is to expand the Green function in terms of a complete orthonormal set $\{\boldsymbol{\xi}(\Gamma_i t)\}$ of basis vectors for the irreducible representations of the point group considered (for the symmetry basis vectors of the irreducible representations see Ludwig (1964)):

$$\mathbf{G} = \sum_{itt'} \boldsymbol{\xi}(\Gamma_i t)G_{\mathrm{B}}(\Gamma_i tt')\boldsymbol{\xi}^{\mathrm{T}}(\Gamma_i t') \qquad G_{\mathrm{B}}(\Gamma_i tt') := \boldsymbol{\xi}^{\mathrm{T}}(\Gamma_i t)\mathbf{G}\boldsymbol{\xi}(\Gamma_i t') \tag{5}$$

where $\Gamma_i$ denotes the representation and $t$ labels the vectors within a representation.

The final result is

$$i_{\alpha\gamma,\beta\lambda}(-|\omega|) = \frac{1}{\pi}\hbar\eta(\omega)\,\mathrm{Im}\left(\sum_{itt'} \mathcal{P}^{\mathrm{T}}_{\alpha\gamma}\boldsymbol{\xi}(\Gamma_i t)G_{\mathrm{B}}(\Gamma_i tt')\mathcal{P}_{\beta\lambda}\boldsymbol{\xi}^{\mathrm{T}}(\Gamma_i t')\right) \tag{6}$$

where the index $i$ refers to the Raman-active representations listed in table 1.

Now we suppose that only those constants $\mathcal{P}_{\alpha\beta}(m)$ are appreciably different from zero in which $m$ refers to an atom in the neighbourhood of the defect or the defect pair. In our case we consider only atoms which are, at the most, nearest, second or fourth neighbours.

A remark should be made concerning equation (6). $\mathbf{G}$ denotes the Green function matrix of the perturbed crystal. Knowledge of the mass change and the force constant changes allows the calculation of the perturbed Green function from the unperturbed one by the Lifshitz technique:

$$\mathbf{G}(z) = [\mathbf{1} + \mathbf{G}_0(z)\mathbf{C}(z)]^{-1}\mathbf{G}_0(z). \tag{7}$$

**C** is the defect matrix, $\mathbf{C}(z) = (\mathbf{\Phi} - \mathbf{\Phi}_0) - z(\mathbf{M} - \mathbf{M}_0)$, where $\mathbf{\Phi}$ and $\mathbf{\Phi}_0$ are the matrices containing the force constants, and **M** and $\mathbf{M}_0$ are the matrices containing the masses of the perturbed and the unperturbed system, respectively. In § 4, we give the details of the force constant changes considered and the calculations.

## 4. Numerical calculations and results

We have calculated the spectra for the NaCl crystal doped with 3% KCl and for the KCl crystal doped with 6% NaCl. If one assumes a statistical distribution of the impurities, most of the defects will find no other defects in their neighbourhood or at best will have an impurity ion at a second- or fourth-neighbour site. Therefore we have calculated the contributions of single defects as well as of defect pairs (in the [100] and the [110] direction) to the spectra. Multiplication with the appropriate concentrations is equivalent to the so-called average $T$-matrix aproximation; see, e.g., Elliott and Leath (1975).

### *4.1. The unperturbed Green function*

The unperturbed Green function is calculated from the breathing shell model (Nüsslein and Schröder 1967). The macroscopic input data for this model are given in table 2. The unperturbed frequencies and eigenvectors are evaluated for 1686 $q$-vectors in the one-fortyeighth section of the Brillouin zone. This is equivalent to 64000 $q$-vectors in the whole Brillouin zone. The imaginary part of the Green function is obtained by calculating first a histogram of 100 bins between $z = 0$ and $z = \omega^2_{\max}$ and then connecting the midpoints of the bins by straight-line segments. The real part of the Green function is obtained by the Kramers–Kronig relation

$$\mathrm{Re}[G(\Gamma_i; \omega^2)] = \frac{1}{\pi} P \int_0^{\omega^2_{\max}} \mathrm{d}z \, \frac{\mathrm{Im}[G(\Gamma_i; z)]}{z - \omega^2}.$$

In view of the fact that also polarisation-dependent photon–phonon coupling constants and inter-shell force constant changes will be investigated, core and shell degrees of

**Table 2.** Input data for the breathing shell model.

| Parameter (units) | NaCl | KCl |
|---|---|---|
| $r_0$ (Å) | 2.7978[a] | 3.1223[a] |
| $c_{11}$ ($10^{12}$ dyn cm$^{-2}$) | 0.5733[a] | 0.4832[a] |
| $c_{12}$ ($10^{12}$ dyn cm$^{-2}$) | 0.1123[a] | 0.054[a] |
| $c_{44}$ ($10^{12}$ dyn cm$^{-2}$) | 0.1331[a] | 0.0663[a] |
| $\alpha_1$ ($10^{-24}$ cm$^3$) | 0.290[a] | 1.133[a] |
| $\alpha_2$ ($10^{-24}$ cm$^3$) | 2.946[a] | 2.946[a] |
| $\omega_0$ ($10^{13}$ rad/s) | 3.30[a] | 2.846[c] |
| $\varepsilon_0$ | 5.43[a] | 4.49[c] |
| $\varepsilon_\infty$ | 2.33[b] | 2.20[d] |
| $Z$ | 0.9 | 0.9 |
| $M_1$ (amu) | 22.990 | 39.102 |
| $M_2$ (amu) | 35.4530 | 35.4530 |

[a] Hardy and Karo (1979).
[b] Sherwood (1972).
[c] Lowndes and Martin (1969).
[d] Bilz *et al* (1984).

**Table 3.** Relative force constant changes $D$ and relaxation $R$ (Sangster 1986). Note that $D_{01} = 60\%$ for $NaCl:K^-$ has been used in the spectra shown in figure 7(*b*)–7(*e*).

| | $NaCl:K^+$ | | $KCl:Na^+$ | |
|---|---|---|---|---|
| Ion pair | $D$ (%) | $R$ (%) | $D$ (%) | $R$ (%) |
| Defect and first neighbour | $D_{01} = +66$ | +5.17 | $D_{01} = -49$ | −4.85 |
| First and fourth neighbours | $D_{14} = +36$ | −3.26 | $D_{14} = -25$ | +3.26 |
| First and first neighbours | $D_{11} = -51$ | +5.17 | $D_{11} = +124$ | −4.85 |
| First and second neighbours | $D_{12} = -8$ | +0.93 | $D_{12} = +5$ | −0.57 |

freedom are kept explicit throughout the calculations (Page and Strauch 1967, 1968, Strauch and Page 1968, Strauch 1968).

### *4.2. The defect matrix*

Apart from the mass changes (only for the defect pairs) the defect matrices contain the force constant changes in the perturbed crystal. In our model, only changes in the longitudinal force constants between the shells of near ions are considered. We neglect changes in the transverse constants, because these constants and thus their changes are an order of magnitude smaller than the longitudinal constants. We consider force constant changes $D_{01}$ between (the shells of) the defect and nearest neighbours and force constant changes $D_{11}$ between two nearest neighours. In the case of the single defect (single defects give the strongest contributions to the spectra and therefore should be treated more precisely), we also take into account changes $D_{12}$ between nearest and second neighbours and changes $D_{14}$ between nearest and fourth neighbours.

For a first estimate of the short-range force constant changes for a single defect, we have calculated these changes within the model for inter-ionic potentials in alkali halides of Sangster and Atwood (1978). In this model the specifications are completely in terms of two types of parameter: parameters which relate to the constituent ions; parameters which apply to the whole group of alkali halides.

Our calculations are based on the data for the relaxations in an NaCl and a KCl crystal with a single defect (K and Na, respectively) which have been evaluated by Sangster (1986). These force constant changes, given in table 3, include the changes in the Coulomb forces between the regarded neighbours which are lower by an order of magnitude. Other changes in the Coulomb forces can be neglected.

There is no *a priori* reason why the force constants and their changes within the two models should be the same but, since the force constants lead, among others, to the same elastic constants, they are expected to be similar, at least. After the relative force constants of the Sangster–Atwood potential have been taken over to the breathing shell model, subsequent refinement did not result in any improvement of the calculated spectra, with one marginal exception (see § 4.4). A byproduct seems to be that, although the Sangster–Atwood potential gives inter-ionic force constants somewhat different from the inter-shell force constants of the breathing shell model, the relative defect-induced force constant changes seem to be very similar in both cases.

Because we do not know the relaxation around the defect pairs, we can only estimate the force constant changes in these cases. In a simple model, we assume that they are equal to the corresponding changes in the single-defect configuration.

### *4.3. Coupling constants*

We discuss two possible mechanisms for the change in the crystal polarisability. The 'intra-ionic' polarisability change may depend on the electronic charge deformation of the ions, i.e. in shell model terms on the relative shell displacement (which is the difference between core and shell displacements) at a given site (model A). An alternative is the 'inter-ionic' polarisability change which depends on the relative displacements of neighbouring (ions or) shells (model B). For second-order Raman scattering in pure alkali halides, model B was successful (Krauzman 1973, Haberkorn 1974), while model A applies to covalent crystals (Kunc and Bilz 1976). So it is an obvious assumption that model B is also appropriate for the impurity-induced Raman scattering in those crystals. Nevertheless, we have investigated both models.

For reasons of inversion symmetry (as in the pure crystal) the coupling constants are zero for the defect site; they are expected to be largest for the defect's neighbours and to fall off with increasing distance from the defect (because of decreasing lattice distortion). In practice, we have included coupling constants on (the shells of) the first neighbours in (unsuccessful) model A and out to fourth neighbours in model B (see § 4.4 for details).

An estimate of the coupling constants for the nearest neighbours of the defect from the elasto-optic (Pockels') constants (Maradudin and Burstein 1967) for the unperturbed crystal leads to incorrect ratios between the intensities for the three scattering geometries. Apparently the neighbourhood of an ion pair in the pure crystal is different from that in the perturbed crystal; this would result in different electronic wavefunctions and therefore in different polarisabilities. So we have adjusted the coupling parameters to the experimental spectra.

### *4.4. Results*

In figure 7 the theoretical results for the impurity-induced Raman scattering in $NaCl:K^+$ are compared with experiment and in figure 8 likewise for $KCl:Na^+$. The spectra are separated into the three symmetries $A_{1g}$, $E_g$ and $T_{2g}$ of the point group $O_h$ of a single defect.

Figure 7(*e*) shows the spectrum that one obtains in model A with the assumption that only the coupling constants for the first neighbours are appreciably different from zero. The force constant changes are those calculated from the model of Sangster and Atwood (1978). Comparison with experimental data shows a rather poor agreement which could not be improved by variation in the force constant changes. Serious discrepancies are, for example, the missing peak at 195 $cm^{-1}$ found in the experimental $A_{1g}$ spectrum and the lineshape of the $E_g$ spectrum in the 120–180 $cm^{-1}$ range.

In comparison, the spectrum calculated from model B (figure 7(*b*)) shows a substantial improvement in these regions. Because the spectra of $KCl:Na^+$ calculated from model A also show little agreement with experiment, this confirms our assumption that the 'inter-ionic' polarisability plays the most important part in defect-induced first-order Raman scattering as it does in second-order scattering in the pure crystal.

In the calculation employing model B, we have used a change of 60% instead of 66% (as in table 3) for the force constant changes between defect and nearest neighbours, because this leads to slightly better results.

By taking into account non-zero coupling constants for second and fourth neighbours the agreement of the theoretical with the experimental spectra can be further improved.

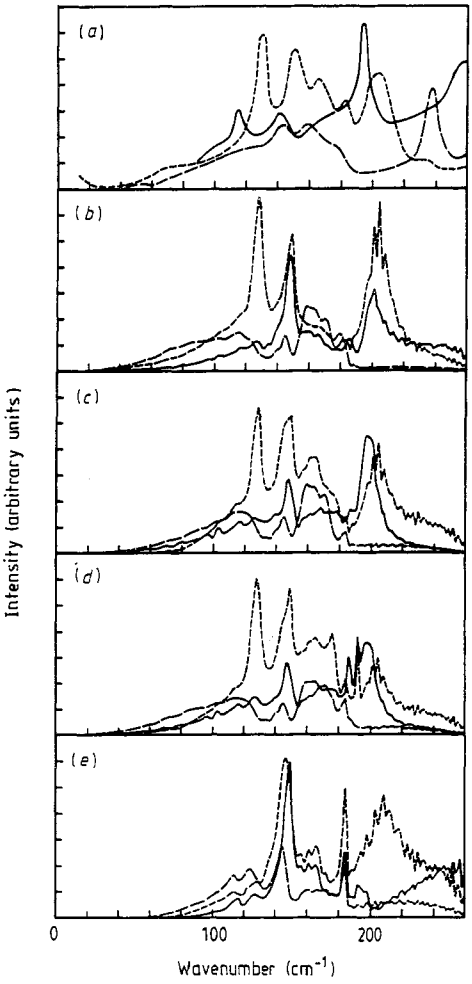


**Figure 7.** Defect-induced spectra of $A_{1g}$ (——), $\frac{3}{4}E_g$ (-----) and $\frac{1}{2}T_g$ modes (---) for NaCl:$K^+$ (the parameters are given in tables 3 and 4). (*a*) experimental spectrum (note that the two-phonon background of the experimental spectra has not been subtracted); (*b*) theoretical spectrum using model B with single defects and coupling constants extending to first neighbours of the defect; (*c*) same as (*b*) but with coupling constants extending to first, second and fourth neighbours; (*d*) same as (*c*) but additionally including the spectra of defect pairs with coupling constants extending to first neighbours of each of the defect-pair atoms; (*e*) same as (*b*) but using model A.

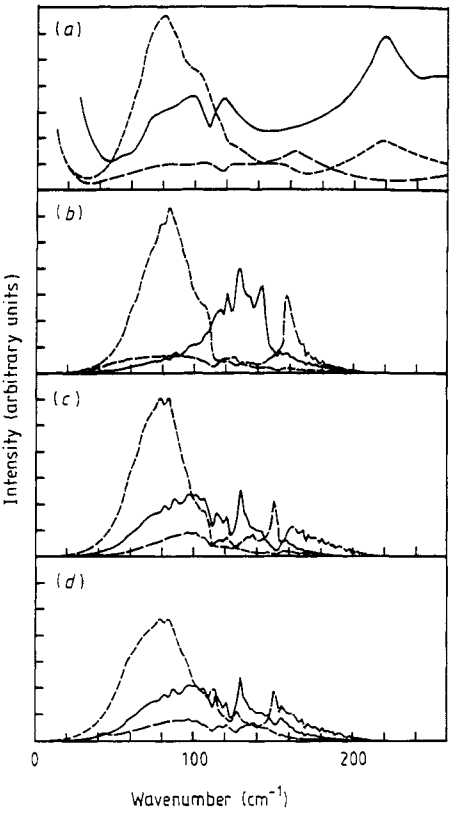


**Figure 8.** Same as figure 7 but for KCl:$Na_+$.

To begin with, we have kept the values of the coupling parameters $P_{\alpha\beta}(1\gamma)$ from the first-neighbour fit and added and adjusted $P_{\alpha\beta}(2\gamma)$ and $P_{\alpha\beta}(4\gamma)$. Subsequent readjustment of $P_{\alpha\beta}(1\gamma)$ did not substantially improve the fit; so we have kept its original value.

The results are given in figure 7(*c*). There still remain two serious discrepancies which should be noted. In the $A_{1g}$ spectrum the prominent peak at 110 $cm^{-1}$ cannot be

**Table 4.** Coupling parameters $P_{\alpha\beta}(m\gamma)$ (up to a common factor) of first, second and fourth neighbours with $m \triangleq 1 = (\frac{1}{2}, 0, 0)a$, $m \triangleq 2 = (\frac{1}{2}, \frac{1}{2}, 0)a$ with $m = 4 \triangleq (1, 0, 0)a$, respectively.

| $P_{\alpha\beta}(m\gamma)$ | $NaCl:K^+$ | $KCl:Na^+$ |
|---|---|---|
| $P_{xx}(1x)$ | 1.000 | 1.000 |
| $P_{yy}(1x)$ | −0.038 | −0.038 |
| $P_{xy}(1y)$ | −0.330 | −0.330 |
| $P_{xx}(2x)$ | −0.048 | −0.068 |
| $P_{yy}(2x)$ | 0.198 | −0.068 |
| $P_{zz}(2x)$ | 0.050 | −0.068 |
| $P_{xy}(2x)$ | 0.000 | 0.000 |
| $P_{xz}(2z)$ | 0.060 | 0.243 |
| $P_{xx}(4x)$ | 0.000 | 0.475 |
| $P_{yy}(4x)$ | 0.000 | 0.250 |
| $P_{xy}(4y)$ | 0.000 | 0.000 |

reproduced in our theory. Moreover, the intensity of the calculated spectrum is too low over the whole frequency range up to 140 $cm^{-1}$. In the $T_{2g}$ spectrum the double-peak structure is not well reproduced. There is a peak which corresponds to the high-frequency part of the double peak, but in the range between 120 and 150 $cm^{-1}$ there is far too little intensity in our calculated spectrum.

Figure 8 gives the results for the KCl crystal with $Na^+$ defects. Again one sees that one can achieve better agreement with experiment by assuming non-zero coupling coefficients for the second and fourth neighbours. As far as the spectra of $KCl:Na^+$ are concerned, one should bear in mind that the relatively high defect concentration (6%) leads to broadening. Furthermore, all the experimental spectra show defect-induced scattering intensity above the one-phonon cut-off at 216 $cm^{-1}$. As mentioned in § 2, this is certainly not first-order Raman scattering. So only the range below the one-phonon cut-off should be compared with theory. The theoretical $KCl:Na^+$ spectra show better agreement with the experimental data than the $NaCl:K^+$ spectra do. However, the theoretical $A_{1g}$ peak at 130 $cm^{-1}$ is 9 $cm^{-1}$ above the experimental peak. The peak in the calculated $T_{2g}$ spectrum at 152 $cm^{-1}$ does not appear in the experiment; there is also too little intensity in the low-frequency range.

Figures 7(*d*) and 8(*d*) show the spectra that one obtains by taking into account the contribution of the defect pairs, assuming statistical distributions. We have also restricted force constant changes and coupling parameters to the important ones, i.e. out to nearest neighbours. Not knowing any better, we have used the same numerical values as obtained from the previous fits using single defects, these giving the essential features, anyway. As a result, inclusion of defect pairs does not remove the serious discrepancies in the $A_{1g}$ and $T_{2g}$ spectrum of $NaCl:K^+$; they only affect the higher-frequency part of the spectra. Improvements are seen in parts of the $E_g$ spectrum of $NaCl:K^+$ and of $KCl:Na^+$, in parts of the $T_{2g}$ spectrum of $KCl:Na^+$, whereas worsening is found in the $A_{1g}$ spectrum.

Our theoretical results could not be improved by variation in the force constant changes. Every improvement in one scattering geometry is parallelled by a serious worsening in another one. So the above spectra presented in figure 7(*c*) and 8(*c*) are those with the best overall agreement. The missing peak in the $A_{1g}$ spectrum of $NaCl:K^+$ possibly suggests that there are still other defects in the crystal, but a comparison with previous investigations of defects in NaCl (Kaiser and Möller 1969, Möller and Kaiser 1972) gives no hints as to the identify of such a possible defect.

As a final conclusion, one can say that because of the serious discrepancies in the spectra of NaCl:$K^+$ compared with experiment there is much reason for criticism. The spectra of KCl:$Na^+$ show better agreement if one considers a certain broadening resulting form the high defect concentration.

## Acknowledgments

The communication of results for the lattice relaxation by Dr M J L Sangster is gratefully acknowledged. This work was supported in part by the National Science Foundation under Grants DMR 82-11857 and 87-06416.

## References

Barker A S and Sievers A J 1975 *Rev. Mod. Phys. Suppl.* 2 **47** S1
Benedek G and Nardelli G F 1967 *Phys. Rev.* **154** 872
Bilz H, Strauch D and Wehner R K 1984 *Handbuch der Physik* vol 25/2d, ed. S Flügge (Heidelberg: Springer)
Born M and Huang K 1954 *Dynamical Theory of Crystal Lattices* (Oxford: OUP)
Elliott R J and Leath P L 1975 *Dynamical Properties of Solids* vol 2, ed. G K Horton and A A Maradudin (Amsterdam: North-Holland)
Haberkorn R 1974 unpublished
Hardy J R and Karo A M 1979 *The Lattice Dynamics and Statics of Alkali Halide Crystals* (New York: Plenum)
Harley R T, Page J B and Walker C T 1971 *Phys. Rev.* B **3** 1365
Höner zu Siederdissen J 1976 *Phys. Status Solidi* b **73** 239
Kaiser R and Möller W 1969 *Phys. Lett.* **28A** 619
Krauzman M 1973 *Solid State Commun.* **12** 157
Kunc K and Bilz H 1976 *Solid State Commun.* **19** 1027
Lowndes R P and Martin D H 1969 *Proc. R. Soc.* A **308** 473
Ludwig W 1964 *Zur Dynamik von Kristallen mit Punktdefekten, Ergebnisse der Exakten Naturwissenschaften* vol 35, ed. S Flügge and F Trendelenburg (Berlin: Springer)
Maradudin A A 1966 *Solid State Phys.* **19** 1 (New York: Academic)
Maradudin A A and Burstein E 1967 *Phys. Rev.* **164** 1081
Möller W and Kaiser R 1972 *Phys. Status Solidi* b **50** 155
Nair I R and Walker C T 1973 *Phys. Rev.* B **7** 2740
Nüsslein V and Schröder U 1967 *Phys. Status Solidi* **21** 309
Page J B and Strauch D 1967 *Phys. Status Solidi* **24** 469
—— 1968 *Localized Excitations in Solids* ed. R F Wallis (New York: Plenum) p 559
Sangster M J L 1986 private communication
Sangster M J L and Atwood R M 1978 *J. Phys. C: Solid State Phys.* **11** 1541
Sherwood P M A 1972 *Vibrational Spectroscopy of Solids* (Cambridge: CUP)
Strauch D 1968 *Phys. Status Solidi* **30** 495
Strauch D and Page J B 1968 *Localized Excitations in Solids* ed. R F Wallis (New York: Plenum) p 567